JACS
JOURNAL OF THE AMERICAN CHEMICAL SOCIETY
Article
pubs.acs.org/JACS

The Effect of Surface Coating on Energy Migration-Mediated Upconversion

Qianqian Su,[†] Sanyang Han,[†] Xiaoji Xie,[†] Haomiao Zhu,[‡] Hongyu Chen,[§] Chih-Kai Chen,[∥] Ru-Shi Liu,[∥] Xueyuan Chen,[‡] Feng Wang,*[,⊥] and Xiaogang Liu*[,†,#]

[†]Department of Chemistry, National University of Singapore, 3 Science Drive 3, Singapore 117543, Singapore

[‡]Key Laboratory of Optoelectronic Materials Chemistry and Physics, Fujian Institute of Research on the Structure of Matter, Chinese Academy of Sciences, Fuzhou, Fujian 350002, China

[§]Division of Chemistry and Biological Chemistry, Nanyang Technological University, Singapore 637371, Singapore

[∥]Department of Chemistry, National Taiwan University, Taipei 106, Taiwan, Republic of China

[⊥]Department of Physics and Materials Science, City University of Hong Kong, 83 Tat Chee Avenue, Hong Kong SAR, China

[#]Institute of Materials Research and Engineering, 3 Research Link, Singapore 117602, Singapore

Supporting Information

ABSTRACT: Lanthanide-doped upconversion nanoparticles have been the focus of a growing body of investigation because of their promising applications ranging from data storage to biological imaging and drug delivery. Here we present the rational design, synthesis, and characterization of a new class of core−shell upconversion nanoparticles displaying unprecedented optical properties. Specifically, we show that the epitaxial growth of an optically inert $NaYF_4$ layer around a lanthanide-doped $NaGdF_4$@$NaGdF_4$ core−shell nanoparticle effectively prevents surface quenching of excitation energy. At room temperature, the energy migrates over Gd sublattices and is adequately trapped by the activator ions embedded in host lattices. Importantly, the $NaYF_4$ shell-coating strategy gives access to tunable upconversion emissions from a variety of activators (Dy^{3+}, Sm^{3+}, Tb^{3+}, and Eu^{3+}) doped at very low concentrations (down to 1 mol %). Our mechanistic investigations make possible, for the first time, the realization of efficient emissions from Tb^{3+} and Eu^{3+} activators that are doped homogeneously with Yb^{3+}/Tm^{3+} ions. The advances on these luminescent nanomaterials offer exciting opportunities for important biological and energy applications.

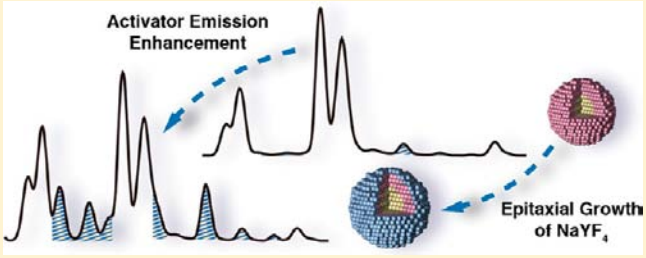

INTRODUCTION

A central goal in biology and medicine is to develop new imaging probes and technologies that enable monitoring of physiological processes in living cells, tissues, and organisms with high spatial resolution. Over the past decade, the development of nanoparticle research has resulted in a great deal of information about imaging probes available with considerable potential for biological researchers.[1,2] Examples include metal nanoparticles with ultrahigh extinction coefficients for labeling in colorimetric assays and quantum dots exhibiting stable, widely tunable fluorescence. These nanostructured biological probes, which are readily amenable to surface bioconjugation, can provide substantially enhanced signals with nanometer resolution. Lanthanide-doped upconversion nanoparticles represent another important, growing class of imaging probes being developed as an alternative to conventional luminescent labels.[3] By comparison, these upconversion nanoparticles offer sharp emission peaks, large anti-Stokes shifts, long-lived excited electronic states, and high photostability.[4]

In recent years, considerable efforts have been devoted to tuning upconversion emissions over a broad spectral range for applications in multicolor labeling and multiplexed biodetection.[5] The strategies for tuning the color output of upconversion nanoparticles typically involve manipulating dopant/host combinations and dopant concentrations.[6,7] For example, $NaYF_4$ nanoparticles doped with different lanthanide activators (Er^{3+}, Ho^{3+}, and Tm^{3+}) show tunable spectra covering the visible and near-infrared region. Spectral lines are the result of electronic transitions within enormously complex energy levels of the lanthanide ions.[8] Notably, $NaYF_4$ and $KMnF_3$ nanoparticles singly doped with Er^{3+} display dramatically different emission profiles due to distinct energy transfer pathways caused by different dopant−host interactions.[9] It is worth noting that the tunable optical emission demonstrated in these nanoparticles is readily reproducible in their corresponding bulk counterparts.

Received: November 12, 2012
Published: December 4, 2012

dx.doi.org/10.1021/ja3111048 | J. Am. Chem. Soc. 2012, 134, 20849−20857

Alternatively, upconversion multicolor fine-tuning can be achieved by utilizing core−shell nanostructures. For example, we previously showed that through use of Gd-mediated energy migration and core−shell engineering, efficient upconversion emission is possible for lanthanide activators (Tb^{3+}, Eu^{3+}, Dy^{3+}, and Sm^{3+}) without long-lived intermediary energy states.[10] The core−shell structure separates the Yb/Tm pair from the activators and eliminates deleterious cross-relaxation. The excitation energy migrates over the Gd sublattice for a substantial distance to the activators, which are confined in the shell layer.[10]

Despite being the conduit to a wide range of activators, our previous core−shell design suffers from limited conversion of the migrating energy stored in Gd sublattices to radiative activator emission.[10] This can be attributed to dominant surface quenching effects.[11] In general, the energy transfer from Gd^{3+} to the activator competes with the energy trapping by surface defects, unknown impurities, passivating ligands, and solvent molecules (Scheme 1). Depending on the nature and concentration of the activators employed, nonradiative dissipation of absorbed excitation energy by surface quenchers can occur. To suppress the energy migration to the surface quenching sites, a feasible solution is to increase the doping concentration of the activators. However, an elevated doping level inevitably results in localized concentration quenching of activator emissions by virtue of enhanced cross-relaxation between the activator ions.

Scheme 1. Schematic Illustration of the Energy Transfer Mechanism in the Core−Shell and $NaYF_4$-Coated Core−Shell−Shell Nanoparticles[a]

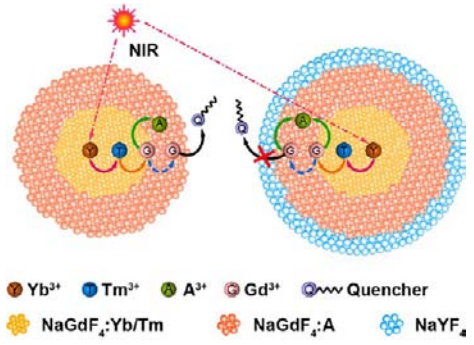

[a]NIR denotes near-infrared irradiation.

In this work, we describe the synthesis and characterization of a series of Gd-based core−shell nanoparticles coated with an optically inert layer of $NaYF_4$. We correlate optical measurements from diverse experiments within activator types (Dy^{3+}, Sm^{3+}, Tb^{3+}, and Eu^{3+}), related experiments involving different dopant concentrations, and all data obtained with a varied thickness of Y^{3+} layer. Together, these efforts reveal the mechanism that dictates the energy migration from the lanthanide sensitizers to the activators. By developing the core−shell process, we found that surface quenching of the migrating energy can be largely suppressed (Scheme 1). This process allows for maximized energy trapping by the activators and thus permits enhanced upconversion emissions even for activators at very low concentrations.

EXPERIMENTAL SECTION

General. Gadolinium(III) acetate hydrate (99.9%), yttrium(III) acetate hydrate (99.9%), ytterbium(III) acetate hydrate (99.9%), thulium acetate hydrate (99.9%), dysprosium(III) acetate hydrate (99.9%), samarium(III) acetate hydrate (99.9%), terbium(III) acetate hydrate (99.9%), europium acetate hydrate (99.9%), sodium hydroxide (NaOH, >98%), ammonium fluoride (NH_4F, >98%), 1-octadecene (90%), oleic acid (90%), dimethyl sulfoxide (DMSO), phosphate buffered saline (PBS) were all purchased from Sigma-Aldrich and used as received unless otherwise noted.

Physical Measurements. Low-resolution transmission electron microscopy (TEM) measurements were carried out on a JEOL-JEM 2010F field emission transmission electron microscope operated at an acceleration voltage of 200 kV. The energy-dispersive X-ray (EDX) spectroscopic analysis was performed with an Oxford INCA energy system operated at 200 kV. High-resolution TEM images were recorded using a JEOL-JEM 3010 transmission electron microscope operated at an acceleration voltage of 300 kV. Powder X-ray diffraction (XRD) data were recorded on a Bruker D8 Advance diffractometer using graphite-monochromatized CuKα radiation (λ = 1.5406 Å). Luminescence spectra were recorded at room temperature with a DM150i monochromator equipped with a R928 photon counting photomultiplier tube (PMT), in conjunction with a 980 nm diode laser. Unless otherwise specified, the emission spectra were normalized to maximum Tm^{3+} emission at 450 nm. All spectra were collected under identical experimental conditions. The decay curves were measured with a customized ultraviolet to mid-infrared steady-state and phosphorescence lifetime spectrometer (FSP920-C, Edinburgh) equipped with a digital oscilloscope (TDS3052B, Tektronix) and a tunable midband OPO laser as the excitation source (410−2400 nm, Vibrant 355II, OPOTEK). The effective decay time τ_{eff} is calculated by

$$\tau_{\text{eff}} = \frac{1}{I_0}\int_0^\infty I(t)\mathrm{d}t$$

where $I(t)$ denotes the luminescence intensity as a function of time t and I_0 represents the maximum intensity. Upconversion luminescence microscopy was performed on an Olympus BX51 microscope with the xenon lamp adapted to a 980 nm diode laser. Luminescence micrographs were recorded with a Nikon DS-Ri1 imaging system. Digital photographs were taken by a Nikon D700 camera.

Synthesis of $NaGdF_4$:Yb/Tm Core Nanoparticles. Yb/Tm codoped $NaGdF_4$ nanoparticles were prepared according to a literature procedure.[10] $Gd(CH_3CO_2)_3$ (0.067 g; 0.2 mmol), $Yb(CH_3CO_2)_3$ (0.069 g; 0.196 mmol), and $Tm(CH_3CO_2)_3$ (0.001 g; 0.004 mmol) dissolved in a water solution (2 mL) were combined at room temperature in a 50 mL two-neck round-bottom flask charged with oleic acid (4 mL). The resulting mixture was then heated at 150 °C for 30 min to remove the water solvent, followed by the injection of 1-octadecene (6 mL). The mixture was stirred at 150 °C for another 30 min before cooling down to 50 °C. Subsequently, a methanol solution (5.4 mL) of NH_4F (0.05 g; 1.36 mmol) and NaOH (0.04 g; 1 mmol) was added and stirred for 30 min. The reaction mixture was then heated at 100 °C for 30 min *in vacuo* to remove the methanol. After purging with argon, the solution was heated to 290 °C and kept for 1.5 h before cooling down to room temperature. The as-prepared nanoparticles were precipitated by addition of ethanol, collected by centrifugation at 6000 rpm for 5 min, and washed with ethanol for several times. The core nanoparticles are stored in cyclohexane (3 mL) prior to being used for shell coating.

Synthesis of $NaGdF_4$:Yb/Tm@$NaGdF_4$:A (A = Dy, Sm, Tb, Eu) Core−Shell Nanoparticles. The preparation of core−shell nanoparticles was developed via a modified literature procedure.[10] The presynthesized $NaGdF_4$:Yb/Tm core nanoparticles were used as seeds for shell modification. In a typical experiment, the shell stock solution was first prepared by mixing water solutions (2 mL each) of $Gd(CH_3CO_2)_3$ (0.132 g; 0.396 mmol) and $A(CH_3CO_2)_3$ (0.001 g; 0.004 mmol; A = Dy, Sm, Tb, Eu) in a 50 mL flask containing 4 mL of oleic acid. The resulting mixture was heated at 150 °C for 30 min, at which time 1-octadecene (6 mL) was added and kept for another 30

dx.doi.org/10.1021/ja3111048 | J. Am. Chem. Soc. 2012, 134, 20849−20857

min before cooling down to 50 °C. A cyclohexane dispersion (3 mL) of $NaGdF_4$:Yb/Tm nanoparticle seeds was then added along with NH_4F (0.05 g; 1.36 mmol) and NaOH (0.04 g; 1 mmol). The reaction was stirred at 50 °C for 30 min and then heated to 290 °C under an argon atmosphere. The high-temperature heating continued for 1.5 h before cooling down to room temperature. The resulting core−shell nanoparticles were collected by addition of ethanol and washed with ethanol for several times before being dispersed in cyclohexane.

Synthesis of $NaGdF_4$@$NaGdF_4$@$NaYF_4$ and $NaGdF_4$@$NaGdF_4$@$NaGdF_4$ Multilayered Nanoparticles. Multilayered core−shell nanoparticles were synthesized using a procedure similar to the one for core−shell nanoparticles. The $NaGdF_4$@$NaGdF_4$ core−shell nanoparticles were used as seeds and conformally coated with a thin layer of $NaGdF_4$ or $NaYF_4$. The $NaYF_4$ shell precursor was prepared by mixing $Y(CH_3CO_2)_3$ (0.052 g, 0.2 mmol), 3 mL of oleic acid, and 7 mL of 1-octadecene in a 50 mL flask followed by heating at 150 °C for 60 min before cooling down to 50 °C. Note that the final-step heat treatment was undertaken at 280 °C.

Synthesis of $NaGdF_4$:Yb/Tm@$NaYF_4$Core−Shell Nanoparticles. The synthetic procedure for $NaGdF_4$:Yb/Tm@$NaYF_4$ nanoparticles was identical to that for $NaGdF_4$:Yb/Tm@$NaGdF_4$ nanoparticles except for the use of a shell stock solution of $NaYF_4$ and a final-step heat treatment at 280 °C.

Synthesis of $NaGdF_4$:Yb/Tm@$NaYF_4$@$NaYF_4$:Tb Nanoparticles with Multilayered $NaYF_4$ Shells. The preparation of core−shell nanoparticles with multilayered $NaYF_4$ shells follows the typical process for making $NaGdF_4$:Yb/Tm@$NaYF_4$ nanoparticles. For a layer-by-layer coating process to proceed, the $NaGdF_4$:Yb/Tm core nanoparticles were treated with different amounts of $NaYF_4$ precursor (5 mL added for each layer). The outermost layer of $NaYF_4$:Tb was first prepared using a stock solution containing $Y(CH_3CO_2)_3$ (0.045 g; 0.17 mmol), $Tb(CH_3CO_2)_3$ (0.01 g; 0.03 mmol), oleic acid (3 mL), and 1-octadecene (7 mL). The reaction was heated in a 50 mL flask at 150 °C for 60 min before cooling down to 50 °C. Subsequently, $NaGdF_4$:Yb/Tm nanoparticles coated with different layers of undoped $NaYF_4$ were added to the flask, together with a methanol solution (3 mL) of NH_4F (0.03 g; 0.8 mmol) and NaOH (0.02 g; 0.5 mmol). Note that the heat treatment for each successive coating of $NaYF_4$ layers was all carried out at 280 °C.

Synthesis of Ligand-Free Nanoparticles. Ligand-free nanoparticles were obtained according to a modified literature procedure.[12] The oleic acid-capped nanoparticles were dispersed in a hydrochloric acid solution (1 mL; 2 M) and ultrasonicated for 5 min to remove the surface ligands. The resulting products were collected by centrifugation at 16 500 rpm for 20 min, washed with ethanol for several times, and redispersed in deionized water.

Cell Imaging. HepG2 cells were first seeded in culture dishes (35 mm) and cultured for 1 day (5% CO_2, 37 °C) in a Dulbecco's modified eagle's medium (DMEM). Subsequently, the culture medium in was replaced by a fresh DMEM medium (1 mL) containing ligand-free nanoparticles (100 μg). The HepG2 cells were then incubated with the nanoparticles for 2 h (5% CO_2, 37 °C). After washing with a PBS buffer solution, the nanoparticle-treated cells were imaged under the irradiation of a 980 nm laser.

RESULTS AND DISCUSSION

We began with a cyclohexane solution of presynthesized $NaGdF_4$:Yb/Tm (49/1%) core nanoparticles and successively deposited two shells of $NaGdF_4$:A (A = Dy, Sm, Tb, and Eu, respectively; 1% each) and $NaYF_4$ through an epitaxial growth process (Figure 1). Notably, the layer-by-layer growth process has also been extensively investigated by the groups of Yan, Zhang, Wang, and van Veggel.[13] The as-synthesized multishell nanoparticles were confirmed to be single crystals with a hexagonal phase by high-resolution TEM and XRD studies (Figure S1). The marked enhancement in upconverted emission intensity of activators after surface processing of nanoparticles suggests the shell formation of $NaYF_4$. It should

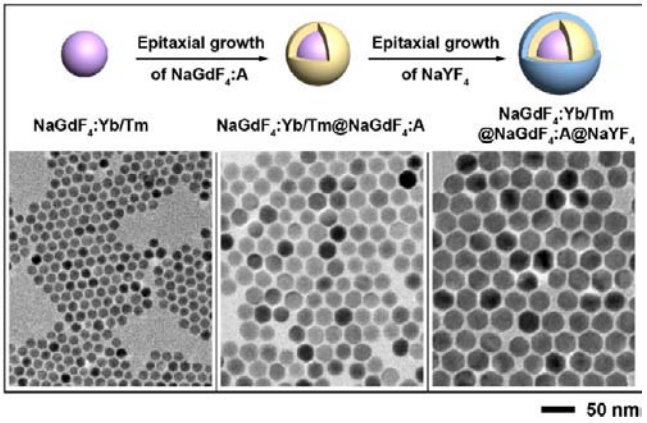

Figure 1. Schematic presentation showing the synthetic process for multishell nanoparticles and TEM images of the as-synthesized nanoparticles.

be noted that during the course of shell coating, phase separation often occurs as a result of kinetically favored nucleation of shell precursors in cubic form, thereby leading to the formation of polydispersed particles. Our controls showed that a relatively low $NaYF_4$ precursor concentration (0.2 mmol; 10 mL) and a high heating temperature of 280 °C proved to be effective for obtaining uniform $NaYF_4$-coated nanoparticles (Figure S2).

We next compared the optical property of the $NaYF_4$-coated nanoparticles with that of previously reported nanoparticles without coating of $NaYF_4$. It should be mentioned that relatively high activator concentrations (5% Dy, 5% Sm, 15% Tb, 15% Eu) are employed in the previous work to give rise to strong upconverted emissions.[10] However, an elevated doping concentration typically causes quenching of activator emission because of the enhanced cross-relaxation between activator ions. Consequently, the activator emissions from higher energy levels can be easily quenched in favor of the emissions resulting from lower energy levels. To suppress the concentration quenching effect and thus enable emissions at high energy levels, the concentration of the activator must be restricted to below a certain threshold. Nevertheless, a low concentration of activator ions (e.g., 1% Tb) resulted in weak emission intensity, particularly that in the UV region (Figure 2, left panel). In contrast, under an identical activator doping condition, we observed remarkably enhanced emission of Tb^{3+}, especially the UV emission from the $^5D_3$ energy level, for $NaYF_4$-coated nanoparticles (Figure 2, right panel). Usually, the Tb emission in the UV range is quenched at high Tb concentrations in favor of the green emission from the $^5D_4$ energy level. Therefore, $^5D_3 \rightarrow {}^7F_J$ (J = 4−6) optical transitions could hardly be spectroscopically detected. The emission enhancement in the visible region from 405 to 635 nm for $NaYF_4$-coated core−shell nanoparticles doped with 1 mol % of Eu^{3+} was also observed. Similarly, with the $NaYF_4$ shell coating, we observed significant emission enhancement for Gd-based nanoparticles doped with a low concentration (1%) of Dy^{3+} and Sm^{3+}, respectively (Figure 2, right panel).

To identify the dominant effect responsible for the enhanced activator emission in $NaGdF_4$:Yb/Tm@$NaGdF_4$:A nanoparticles, we have compared the excited-state lifetimes of Gd^{3+} and Tb^{3+} obtained before and after $NaYF_4$ coating. As shown in Figure 3a, a significant increase (~1.82 times) in Gd^{3+} lifetime ($^6P_{7/2}$) was observed when a $NaYF_4$ shell layer was applied. In

dx.doi.org/10.1021/ja3111048 | J. Am. Chem. Soc. 2012, 134, 20849−20857

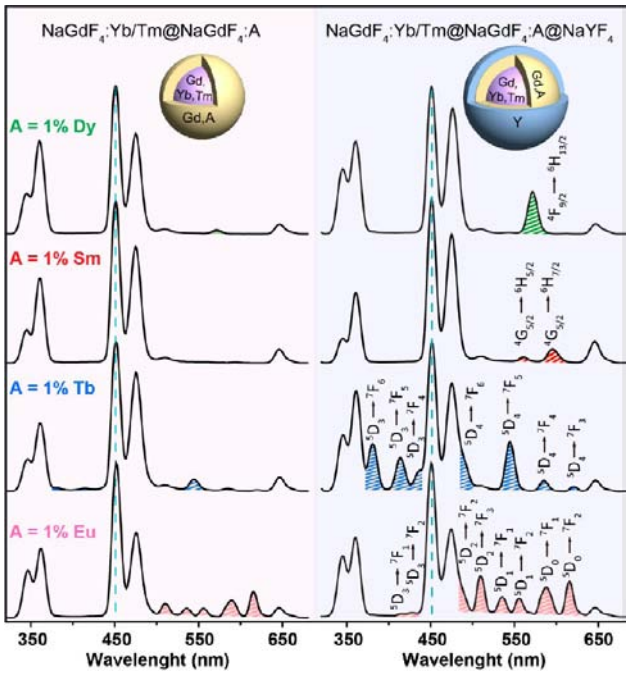

Figure 2. Room-temperature emission spectra of the as-prepared $NaGdF_4$@$NaGdF_4$:A (A = Dy, Sm, Tb, and Eu, respectively; 1% each) and their corresponding $NaYF_4$-modified (~2.5 nm thick) nanoparticles. Note that activator emissions are highlighted with color. All spectra were recorded under excitation of a 980 nm CW diode laser at a power density of 10 W cm^{-2}.

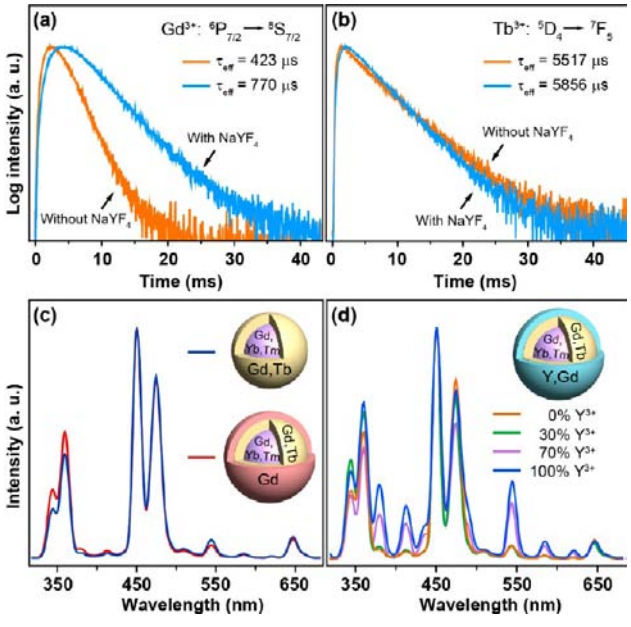

Figure 3. (a,b) Upconversion luminescence decay curves of Gd^{3+} and Tb^{3+} emissions at 310 and 544 nm, respectively, for the Gd-based nanoparticles (Tb^{3+}:1%) with and without the $NaYF_4$ coating. (c) Emission spectra of the Gd-based nanoparticles (Tb^{3+}:1%) obtained with and without the $NaGdF_4$ coating. (d) Emission spectra of the $NaGdF_4$-coated nanoparticles with the outmost Gd^{3+} layer replaced by varied amounts of Y^{3+} (0, 30, 70, 100%).

stark contrast, the activator lifetime (Tb^{3+}:$^5D_4$) is essentially unaltered by the $NaYF_4$ coating (Figure 3b). The enhanced activator emission is clearly ascribed to the suppressed trapping of Gd^{3+} energy by surface ligands or solvent molecules.

To verify the effect of the activator emission enhancement by $NaYF_4$ layer protection, we further investigated a series of $NaGdF_4$:Yb/Tm@$NaGdF_4$:A@$NaGdF_4$ core−shell−shell nanoparticles. The use of $NaGdF_4$ as the outermost shell provides selective protection to the activators, while the Gd excitation energy can migrate through the Gd shell and dissipate through the trapping by the surface defects or solvent molecules. Photoluminescence study depicted in Figure 3c showed that the Tb^{3+} emission in the core−shell−shell nanoparticles was essentially not improved (also see Figure S3). Importantly, when the Gd^{3+} ions in the outermost shell were gradually replaced by optically inert Y^{3+}, a steady enhancement of the activator emission was observed (Figures 3d and S4). Taken together, the results conclusively suggest that the suppression of surface quenching to the Gd^{3+} ions is primarily responsible for the enhanced activator emissions.

In an attempt to probe the role of $NaYF_4$ layer in protecting Gd^{3+} excitation energy, we conducted a set of control experiments to compare the emission intensity and decay curves of Gd^{3+} emission at 310 nm ($^6P_{7/2} \rightarrow {}^8S_{7/2}$) for $NaGdF_4$:Yb/Tm nanoparticles coated with $NaGdF_4$ and $NaYF_4$. The corresponding emission spectra are shown in Figure 4. It should be mentioned that Gd^{3+} should be more

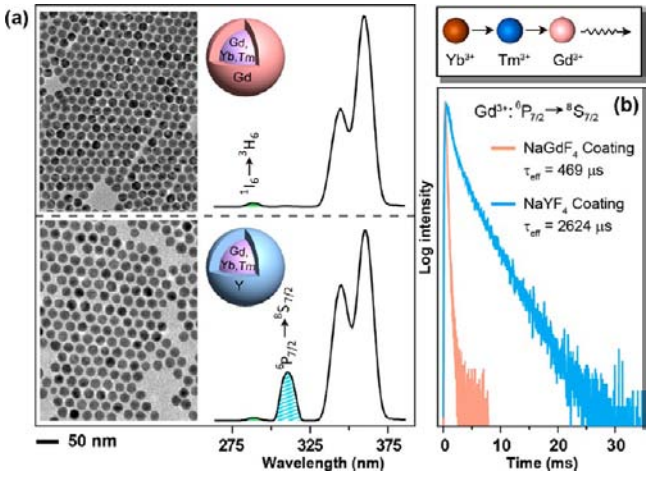

Figure 4. (a) Emission spectra of $NaGdF_4$:Yb/Tm nanoparticles coated with $NaGdF_4$ and $NaYF_4$, respectively. Note that Tm^{3+} ($^1I_6 \rightarrow {}^3S_6$) and Gd^{3+} ($^6P_{7/2} \rightarrow {}^8S_{7/2}$) emissions are highlighted with color and the emission spectra were normalized at 360 nm. (b) Corresponding upconversion luminescence decay curves of Gd^{3+} measured at 310 nm for $NaGdF_4$- and $NaYF_4$-coated core−shell nanoparticles, respectively.

resistant to nonradiative quenching than other lanthanide activator ions, such as Tb^{3+}, Eu^{3+}, Dy^{3+}, and Sm^{3+}, owing to its substantially larger energy gap (~32 200 cm^{-1} from the lowest excited state to the ground state).[14] The strong luminescence quenching of Gd^{3+} in the case of $NaGdF_4$ coating is attributable to rapid energy migration from the gadolinium sublattice to surface quenchers.[15] By comparison, the Gd^{3+} emission in $NaYF_4$-coated nanoparticles was significantly enhanced, clearly indicating that the $NaYF_4$ shell layer could effectively prevent the excitation energy from trapping by the surface quenchers. These results are also consistent with our lifetime decay analysis in that a significantly shorter lifetime (469 μs) of Gd^{3+} emission was recorded for $NaGdF_4$-coated nanoparticles relative to that (2624 μs) of $NaYF_4$-coated counterparts.

dx.doi.org/10.1021/ja3111048 | J. Am. Chem. Soc. 2012, 134, 20849−20857

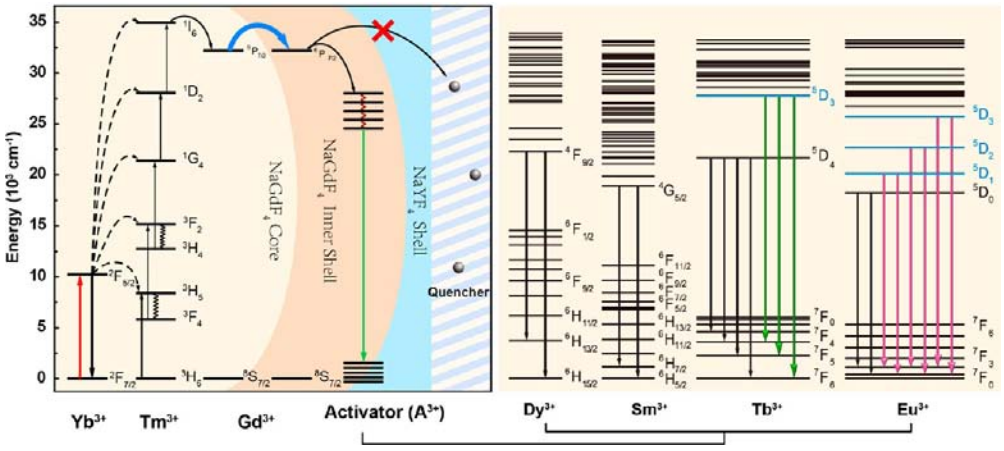

Figure 5. Proposed energy transfer mechanisms in the core−shell−shell nanoparticles. Note that only partial energy levels of Tm^{3+}, Gd^{3+}, and A^{3+} (A = Dy, Sm, Tb, and Eu) are shown for clarity. The optical emissions from higher-lying energy levels of Tb^{3+} and Eu^{3+} are highlighted with colored arrows.

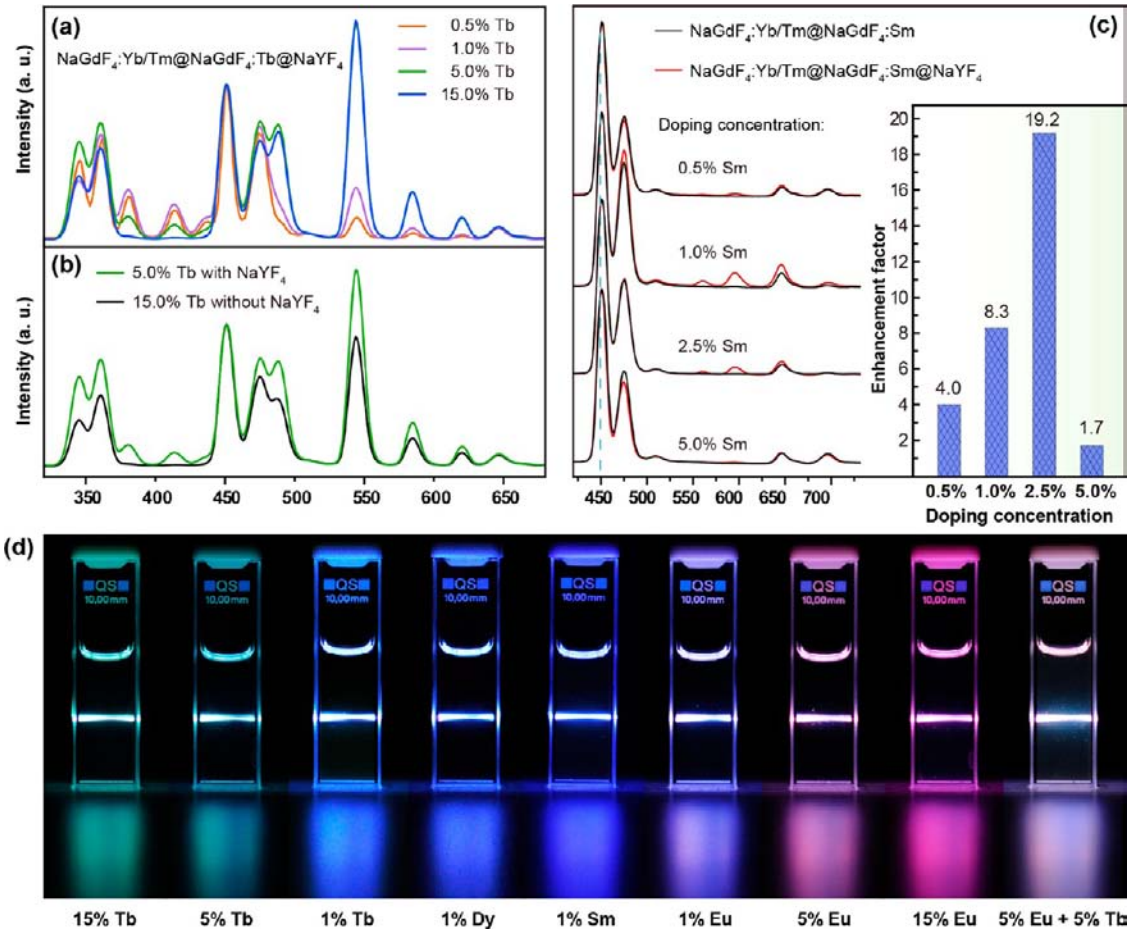

Figure 6. Effect of activator concentration on optical properties of the $NaGdF_4$:Yb/Tm@$NaGdF_4$:A and $NaGdF_4$:Yb/Tm@$NaGdF_4$:A@$NaYF_4$ nanoparticles. (a) Upconversion emission spectra of the Tb^{3+}-doped core−shell−shell nanoparticles as a function of dopant concentration. (b) Comparative spectroscopic studies of the $NaGdF_4$:Yb/Tm@$NaGdF_4$:Tb (15%) with $NaYF_4$-coated $NaGdF_4$:Yb/Tm@$NaGdF_4$:Tb (5%) nanoparticles. (c) Upconversion emission spectra of the as-prepared $NaGdF_4$:Yb/Tm@$NaGdF_4$:Sm and $NaGdF_4$:Yb/Tm@$NaGdF_4$:Sm@$NaYF_4$ nanoparticles obtained with different Sm^{3+} concentrations (inset: enhancement factor of the Sm^{3+} emission obtained by comparing the results for samples with and without the $NaYF_4$ coating. The activator emission intensities were calculated by integrating the spectral intensity of the emission spectra over a wavelength range of 540−620 nm). (d) Luminescence photographs of representative samples in cyclohexane solution (2 mg mL^{-1}) under irradiation of a 980 nm laser.

The influence of shell thickness of $NaYF_4$ on the activator optical emission was subsequently investigated. We observed that the coating of an additional layer (~2.5 nm) of $NaYF_4$ onto the as-prepared core−shell−shell nanoparticles does not

dx.doi.org/10.1021/ja3111048 | J. Am. Chem. Soc. 2012, 134, 20849−20857

lead to further enhancement in activator emission (Figure S6). This was expected as the interaction between dopant ions and surface oscillators typically occurs within a distance of ~3 nm.[16] With a 2.5 nm thick shell of $NaYF_4$, the interaction between the lanthanides and surface ligands or solvent molecules in the surrounding environment is essentially shielded (Figure S6). These results also suggest the integrity of the $NaYF_4$ shell initially coated around the $NaGdF_4$:Yb/Tm@$NaGdF_4$:A.[13f]

We next explored the underlying mechanism that accounts for intense upconversion emission from higher-lying ^5D_J excited states of Tb^{3+} and Eu^{3+} ions (Figure 5). An important prerequisite for the emission from higher-lying energy levels (e.g., $^5D_3$ of Tb^{3+}; $^5D_1$, $^5D_2$, and $^5D_3$ of Eu^{3+}) is the need for $NaGdF_4$ host materials with intrinsic low phonon energy (~350 cm^{-1}). If there are high-frequency vibrations in the host lattices, such as $TbAl_3B_4O_{12}$ (~1300 cm^{-1}) and YBO_3 (~1050 cm^{-1}),[4a,17] the activator emission from the higher-lying energy levels would be readily quenched through multiphonon emission process. Another important factor in satisfying intense activator emission from higher-lying energy levels is the $NaYF_4$ coating that provides efficient trapping of the migrating energy in Gd sublattice. A low doping concentration of activators typically suppresses unwanted cross-relaxation pathways (e.g., $^5D_3 + {}^7F_6 \rightarrow {}^5D_4 + {}^7F_0$ for Tb^{3+} and $^5D_2 + {}^7F_0 \rightarrow {}^5D_0 + {}^7F_5$ for Eu^{3+}) that depopulate the higher-lying energy states of the activators. Furthermore, the $NaYF_4$ shell also enhances activator emission by protecting the activator ions from surface quenching. The higher-lying excited states of Tb^{3+} ($^5D_3$) and Eu^{3+} ($^5D_2$) are highly susceptible to high-energy surface oscillators because of the small energy gap (~5800 and ~1800 cm^{-1}, respectively) to the next lower-lying energy levels (Figure S7).

We found that the enhancement factor varies with changes in activator concentration (Figures 6a and S8). At high activator concentrations, the energy transfer from Gd^{3+} to activator ions dominates energy trapping processes. Thus, the excitation energy of Gd^{3+} will be trapped by the activators before it reaches surface quenching sites. Only marginal enhancement in activator emission is therefore expected through surface protection of nanoparticles. When the activator concentration is substantially decreased, the number of lanthanide trapping centers in nanoparticles becomes insufficient to capture the excessive migrating energy preserved by the $NaYF_4$ shell. Importantly, the $NaYF_4$ shell protection enables stronger upconverted emission of Tb^{3+} doped at a low concentration (5%) as opposed to that of unprotected Tb^{3+} at a high concentration (15%) (Figure 6b).

For Sm^{3+} and Dy^{3+} activators, we noticed that the ability of these two activators to trap the Gd^{3+} energy is quite weak, arising from the presence of many closely spaced energy levels. For example, a Sm^{3+} ion in its $^4G_{5/2}$ excited state may transfer part of its energy to a neighboring ground-state Sm^{3+} ion through cross-relaxation, resulting in both ions occupying the $^6F_{9/2}$ level and subsequent nonradiative relaxation to the ground state. This effect is particularly pronounced at a high Sm^{3+} concentration. Thus, the Sm^{3+} dopant content in nanoparticles has to be kept very low (typically <2.5 mol %). However, weak upconverted emission of Sm^{3+} still occurs in most instances because of inefficient trapping of the migrating energy and surface quenching effect. In our core−shell−shell design, the surface quenching effect can be largely eliminated. Remarkably, we observed more than 1 order of magnitude enhancement in Sm^{3+} emission by coating $NaGdF_4$:Yb/Tm@$NaGdF_4$:Sm nanoparticles with a layer of $NaYF_4$ (Figure 6c). Through the core−shell−shell engineering in nanoparticles, we showed that a wide range of emission colors from ultraviolet to visible can be readily achieved with different types of activators, providing potential implications for the development of multicolored biolabels (Figure 6d).

By analyzing available optical data on concentration dependence, we can derive the critical distance (R_c) between activators for maximum emission intensity according to Blasse's equation:[18]

$$R_c = 2\left(\frac{3V}{4\pi x_c N}\right)^{1/3}$$

where x_c is the critical activator concentration, N is the number of lattice sites in the unit cell that can be occupied by activator ions, and V is the volume of the unit cell. For hexagonal $NaGdF_4$ (JCPDS 27-0699) with a space group of $P6_3/m$ (Z = 1.5), the cell parameters are a = 6.02 Å and c = 3.60 Å, and the volume of the unit cell is 113.02 $Å^3$. The critical concentration is estimated to be 15% for Tb^{3+} and Eu^{3+} and 1% for Dy^{3+} and Sm^{3+}. Using the above equation, R_c was determined to be about 0.99 nm for Tb^{3+} and Eu^{3+} and 2.43 nm for Dy^{3+} and Sm^{3+}.

We also note a significant benefit of using activators doped at low concentrations. In our previous report,[10] a relatively high activator concentration (>2.5%) is typically required to facilitate trapping of the migrating energy in Gd sublattice. To avoid the deleterious cross-relaxation between the Yb/Tm and activator ions, a core−shell structure of $NaGdF_4$@$NaGdF_4$ is necessary to spatially confine different dopant ions for controlled energy exchange interactions. In this work, the realization of efficient emission at a low concentration of activators through the $NaYF_4$ coating should allow us to simplify structural design of the nanoparticles. For example, we showed that with the $NaYF_4$ shell coating, Tb^{3+} and Eu^{3+} ions homogeneously doped at 1% each along with the Yb/Tm pair in the $NaGdF_4$ host lattice can give rise to a similar emission profile to that of the $NaYF_4$-coated $NaGdF_4$:Yb/Tm@$NaGdF_4$:A (A = Tb or Eu) nanoparticles (Figure 7a). By comparison, without the $NaYF_4$ coating, we did not observe any noticeable activator emission under identical test conditions (Figure 7b).

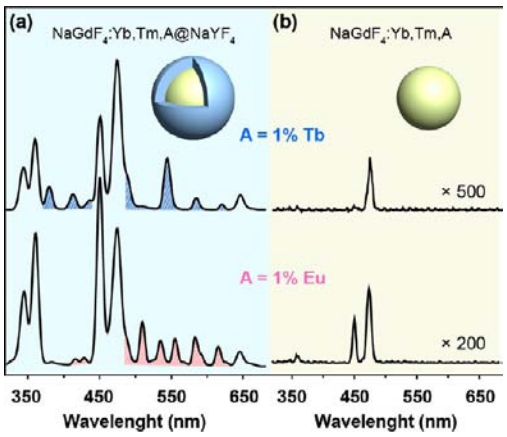

Figure 7. Comparative emission spectra of (a) $NaGdF_4$:Yb/Tm/A@$NaYF_4$ and (b) $NaGdF_4$:Yb/Tm/A nanoparticles with 1% doping level of activators.

dx.doi.org/10.1021/ja3111048 | J. Am. Chem. Soc. 2012, 134, 20849−20857

To further probe the distance for effective energy transfer from Gd^{3+} to Tb^{3+}, we carried out a series of layer-by-layer coating experiments (Figure 8). We precisely controlled the

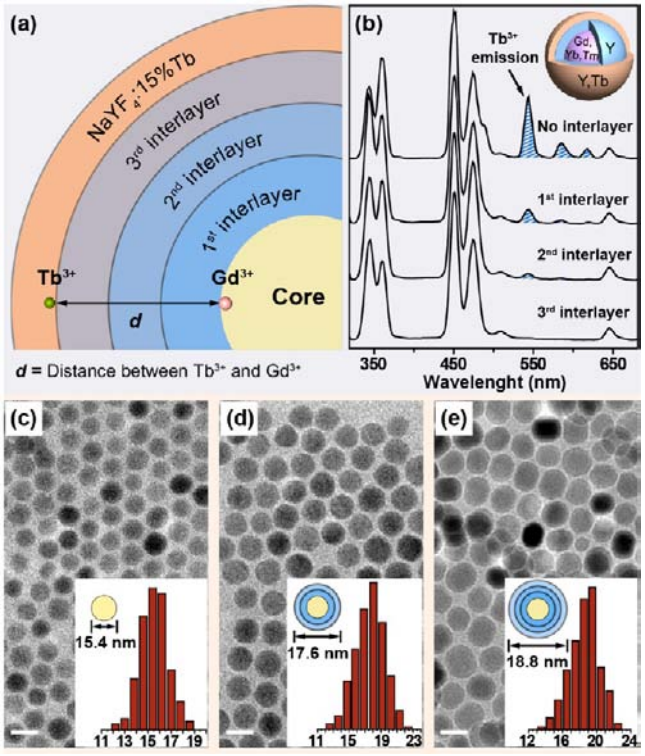

Figure 8. (a) Schematic design of controlling energy transfer from Gd^{3+} to Tb^{3+} through a layer-by-layer growth technique. (b) Emission spectra of the $NaGdF_4$:Yb/Tm@$NaYF_4$@$NaYF_4$:Tb nanoparticles with different thickness of $NaYF_4$ interlayer. (c–e) Corresponding TEM images of the as-prepared nanoparticles (insets are histograms of the particle size distribution.) Note that each interlayer was prepared using a 5 mL of $NaYF_4$ precursor.

spacing (d = 0, 0.5, 1.1, 1.7 nm) between the Gd^{3+} embedded in the nanoparticle core and the Tb^{3+} encapsulated in the $NaYF_4$ shell using optically inert $NaYF_4$ as an interlayer (Figure 8a). The dependence of Tb^{3+} emission on the thickness of the interlayer was shown in Figure 8b. Without the $NaYF_4$ interlayer, we could observe intense Tb^{3+} emission, arising from strong exchange interactions between the Gd^{3+} and Tb^{3+}. After coating of a $NaYF_4$ layer of ~1.1 nm thick (Figure 8d), the emission intensity of Tb^{3+} was significantly reduced. With further increase in the interlayer thickness, the emission of Tb^{3+} gradually decreases and eventually disappears when the interlayer spacing reaches ~1.7 nm. The suppressed Tb^{3+} emission in the multishelled nanoparticle largely results from negligible diffusion of dopant ions in the solid-state host lattice, which is consistent with a previous report.[19]

The use of a $NaYF_4$ shell layer for the nanoparticles is likely to significantly improve the signal strength and minimize the impact of solvents, which is essential for their biological applications. To shed light on the optical stability of $NaYF_4$-coated nanoparticles, we transferred the as-prepared nanoparticles into DMSO/ethanol solutions containing different amounts of water. As shown in Figure S9, the relative emission intensities of the $NaYF_4$-coated nanoparticles were virtually unchanged owing to the effective protection of activators by the inert shell. To further highlight the versatility of these $NaYF_4$-coated nanoparticles in biological applications, we demonstrated multicolor cell imaging using different combinations of Tb^{3+} and Eu^{3+} activators incubated with HepG2 cells (Figure S10).

CONCLUSIONS

The comparison of Gd-based upconversion nanoparticles and their $NaYF_4$-coated counterparts has enabled better understanding of energy migration-mediated upconversion processes. Our results demonstrate how the interplay of lanthanide interactions and core–shell nanostructures can be used to control the optical properties of the upconversion nanoparticles. The $NaYF_4$ shell can impede the migrating energy in Gd sublattice from trapping by surface quenchers, thereby promoting energy trapping by the activators. Alongside this, the clearly enhanced emission for various activators (Dy^{3+}, Sm^{3+}, Tb^{3+}, and Eu^{3+}) leads to the conclusion that efficient emissions can be realized from activators doped homogeneously with Yb/Tm ions through the $NaYF_4$ shell protection, provided the activator concentration is kept at a considerably low level. Demonstrating both control and understanding of the energy migration in these nanoparticles should be a key step toward the rational design of lanthanide-based luminescent nanomaterials for advanced biological applications.

ASSOCIATED CONTENT

Supporting Information

Additional experimental details. This material is available free of charge via the Internet at http://pubs.acs.org.

AUTHOR INFORMATION

Corresponding Author

fwang24@cityu.edu.hk; chmlx@nus.edu.sg

Notes

The authors declare no competing financial interest.

ACKNOWLEDGMENTS

This study was supported by the National University of Singapore (R-143-000-427), the Ministry of Education (R-143-000-453), the Singapore-MIT Alliance, and the Agency for Science, Technology, and Research (R-143-000-366). F.W. is grateful to CityU for the start-up grant (nos. 7200317 and 9610257). X.C. and H.Z. acknowledge the financial support from the NSFC (no. 10974200) and the 863 program of MOST, China (no. 2011AA03A407). We thank Dr. Hui Xu, Dr. Runfeng Chen, and Dr. Xiaoyong Huang for helpful discussions.

REFERENCES

(1) (a) Cutler, J. I.; Auyeung, E.; Mirkin, C. A. *J. Am. Chem. Soc.* **2012**, *134*, 1376. (b) Xue, X.; Wang, F.; Liu, X. *J. Mater. Chem.* **2011**, *21*, 13107. (c) Liu, S.; Han, M. *Adv. Funct. Mater.* **2005**, *15*, 961. (d) Fang, X.; Tan, W. *Acc. Chem. Res.* **2010**, *43*, 48. (e) Saha, K.; Agasti, S. S.; Kim, C.; Li, X.; Rotello, V. M. *Chem. Rev.* **2012**, *112*, 2739. (f) Du, J.; Jiang, L.; Shao, Q.; Liu, X.; Marks, R. S.; Ma, J.; Chen, X. *Small* **2012**. DOI: 10.1002/smll.201200811. (g) Xie, X.; Xu, W.; Li, T.; Liu, X. *Small* **2011**, *7*, 1393. (h) Xie, X.; Xu, W.; Liu, X. *Acc. Chem. Res.* **2012**, *45*, 1511. (i) Xia, Y.; Li, W.; Cobley, C. M.; Chen, J.; Xia, X.; Zhang, Q.; Yang, M.; Cho, E. C.; Brown, P. K. *Acc. Chem. Res.* **2011**, *44*, 914. (j) Murphy, C. J.; Gole, A. M.; Stone, J. W.; Sisco, P. N.; Alkilany, A. M.; Goldsmith, E. C.; Baxter, S. C. *Acc. Chem. Res.* **2008**, *41*, 1721. (k) Xue, X.; Wang, F.; Liu, X. *J. Am. Chem. Soc.* **2008**, *130*, 3244. (l) Dreaden, E. C.; Mackey, M. A.; Huang, X.; Kang, B.; El-

Sayed, M. A. *Chem. Soc. Rev.* **2011**, *40*, 3391. (m) Liu, J.; Cao, Z.; Lu, Y. *Chem. Rev.* **2009**, *109*, 1948. (n) Yehl, K.; Joshi, J. P.; Greene, B. L.; Dyer, R. B.; Nahta, R.; Salaita, K. *ACS Nano* **2012**, *6*, 9150. (o) Lee, J.-H.; Kim, G.-H.; Nam, J.-M. *J. Am. Chem. Soc.* **2012**, *134*, 5456. (p) Xu, W.; Xue, X.; Li, T.; Zeng, H.; Liu, X. *Angew. Chem., Int. Ed.* **2009**, *48*, 6849. (q) Li, D.; Song, S.; Fan, C. *Acc. Chem. Res.* **2010**, *43*, 631. (r) Xu, J.; Wang, H.; Liu, C.; Yang, Y.; Chen, T.; Wang, Y.; Wang, F.; Liu, X.; Xing, B.; Chen, H. *J. Am. Chem. Soc.* **2010**, *132*, 11920. (s) Wang, Y.; Chen, G.; Yang, M.; Silber, G.; Xing, S.; Tan, L. H.; Wang, F.; Feng, Y.; Liu, X.; Li, S.; Chen, H. *Nat. Commun.* **2010**, *1*, 87. (t) Verma, A.; Uzun, O.; Hu, Y.; Hu, Y.; Han, H. S.; Watson, N.; Chen, S.; Irvine, D. J.; Stellacci, F. *Nat. Mater.* **2008**, *7*, 588.

(2) (a) Nagaoka, Y.; Chen, O.; Wang, Z.; Cao, Y. C. *J. Am. Chem. Soc.* **2012**, *134*, 2868. (b) Ju, Q.; Tu, D.; Liu, Y.; Li, R.; Zhu, H.; Chen, J.; Chen, Z.; Huang, M.; Chen, X. *J. Am. Chem. Soc.* **2012**, *134*, 1323. (c) Liu, Y.; Zhou, S.; Tu, D.; Chen, Z.; Huang, M.; Zhu, H.; Ma, E.; Chen, X. *J. Am. Chem. Soc.* **2012**, *134*, 15083. (d) Cheng, L.-C.; Huang, J.-H.; Chen, H. M.; Lai, T.-C.; Yang, K.-Y.; Liu, R.-S.; Hsiao, M.; Chen, C. H.; Her, L.-J.; Tsai, D. P. *J. Mater. Chem.* **2012**, *22*, 2244. (e) Bruchez, M., Jr.; Moronne, M.; Gin, P.; Weiss, S.; Alivisatos, A. P. *Science* **1998**, *281*, 2013. (f) Michalet, X.; Pinaud, F. F.; Bentolila, L. A.; Tsay, J. M.; Doose, S.; Li, J. J.; Sundaresan, G.; Wu, A. M.; Gambhir, S. S.; Weiss, S. *Science* **2005**, *307*, 538. (g) Medintz, I. L.; Uyeda, H. T.; Goldman, E. R.; Mattoussi, H. *Nat. Mater.* **2005**, *4*, 435. (h) Wu, X. Y.; Liu, H. J.; Liu, J. Q.; Haley, K. N.; Treadway, J. A.; Larson, J. P.; Ge, N. F.; Peale, F.; Bruchez, M. P. *Nat. Biotechnol.* **2003**, *21*, 41. (i) Larson, D. R.; Zipfel, W. R.; Williams, R. M.; Clark, S. W.; Bruchez, M. P.; Wise, F. W.; Webb, W. W. *Science* **2003**, *300*, 5624. (j) Dubertret, B.; Skourides, P.; Norris, D. J.; Noireaux, V.; Brivanlou, A. H.; Libchaber, A. *Science* **2002**, *298*, 1759. (k) Yu, W. W.; Qu, L. H.; Guo, W. Z.; Peng, X. G. *Chem. Mater.* **2003**, *15*, 2854. (l) Jin, Y.; Gao, X. *Nat. Nanotechnol.* **2009**, *4*, 571. (m) Park, J.; An, K.; Hwang, Y.; Park, J.-G.; Noh, H.-J.; Kim, J.-Y.; Park, J.-H.; Hwang, N.-M.; Hyeon, T. *Nat. Mater.* **2004**, *3*, 891. (n) Patolsky, F.; Zheng, G.; Lieber, C. M. *Nanomedicine* **2006**, *1*, 51.

(3) (a) Wu, S.; Han, G.; Milliron, D. J.; Aloni, S.; Altoe, V.; Talapin, D. V.; Cohen, B. E.; Schuck, P. J. *Proc. Natl Acad. Sci. U.S.A.* **2009**, *106*, 10917. (b) Wang, M.; Mi, C.; Wang, W.; Liu, C.; Wu, Y.; Xu, Z.; Mao, C.; Xu, S. *ACS Nano* **2009**, *3*, 1580. (c) Nam, S. H.; Bae, Y. M.; Park, Y. I.; Kim, J. H.; Kim, H. M.; Choi, J. S.; Lee, K. T.; Hyeon, T.; Suh, Y. D. *Angew. Chem., Int. Ed.* **2011**, *50*, 6093. (d) Liu, Q.; Sun, Y.; Yang, T.; Feng, W.; Li, C.; Li., F. *J. Am. Chem. Soc.* **2011**, *133*, 17122. (e) Jin, J.; Gu, Y.-J.; Man, C. W.-Y.; Cheng, J.; Xu, Z.; Zhang, Y.; Wang, H.; Lee, V. H.-Y.; Cheng, S. H.; Wong, W.-T. *ACS Nano* **2011**, *5*, 7838. (f) Yang, Y.; Shao, Q.; Deng, R.; Wang, C.; Teng, X.; Cheng, K.; Cheng, Z.; Huang, L.; Liu, Z.; Liu, X.; Xing, B. *Angew. Chem., Int. Ed.* **2012**, *51*, 3125. (g) Zeng, S.; Tsang, M.-K.; Chan, C.-F.; Wong, K.-L.; Fei, B.; Hao, J. *Nanoscale* **2012**, *4*, 5118. (h) Gorris, H. H.; Ali, R.; Saleh, S. M.; Wolfbeis, O. S. *Adv. Mater.* **2011**, *23*, 1652. (i) Li, L.; Zhang, R.; Yin, L.; Zheng, K.; Qin, W.; Selvin, P. R.; Lu, Y. *Angew. Chem., Int. Ed.* **2012**, *51*, 6121. (j) Wang, C.; Cheng, L.; Xu, H.; Liu, Z. *Biomaterials* **2012**, *33*, 4872. (k) Zhang, F.; Shi, Q.; Zhang, Y.; Shi, Y.; Ding, K.; Zhao, D.; Stucky, G. D. *Adv. Mater.* **2011**, *23*, 3775. (l) Deng, R.; Xie, X.; Vendrell, M.; Chang, Y.-T.; Liu, X. *J. Am. Chem. Soc.* **2011**, *133*, 20168. (m) Chen, F.; Bu, W.; Zhang, S.; Liu, X.; Liu, J.; Xing, H.; Xiao, Q.; Zhou, L.; Peng, W.; Wang, L.; Shi, J. *Adv. Funct. Mater.* **2011**, *21*, 4285. (n) Idris, N. M.; Gnanasammandhan, M. K.; Zhang, J.; Ho, P. C.; Mahendran, R.; Zhang, Y. *Nat. Med.* **2012**, *18*, 1580. (o) Lu, G.; Li, S.; Hauser, B. G.; Qi, X.; Wang, Y.; Wang, X.; Han, S.; Liu, X.; Duchene, J. S.; Zhang, H.; Zhang, Q.; Chen, X.; Ma, J.; Loo, S. C. J.; Wei, W.; Yang, Y.; Farha, O. K.; Hupp, J. T.; Huo, F. *Nat. Chem.* **2012**, *4*, 310. (p) Yang, J.; Shen, D.; Li, X.; Li, W.; Fang, Y.; Wei, Y.; Yao, C.; Tu, B.; Zhang, F.; Zhao, D. *Chem.—Eur. J.* **2012**, *18*, 13642.

(4) (a) Blasse, G.; Grabmaier, B. C. *Luminescent Materials*; Springer: Berlin, 1994. (b) Auzel, F. *Chem. Rev.* **2004**, *104*, 139. (c) Bünzli, J.-C. G. *Acc. Chem. Res.* **2006**, *39*, 53. (d) Mai, H.; Zhang, Y.; Si, R.; Yan, Z.; Sun, L.; You, L.; Yan, C. *J. Am. Chem. Soc.* **2006**, *128*, 6426. (e) Haase, M.; Schäfer, H. *Angew. Chem., Int. Ed.* **2011**, *50*, 5808. (f) Wang, F.; Liu, X. *Chem. Soc. Rev.* **2009**, *38*, 976. (g) Zou, W.; Visser, C.; Maduro1, J. A.; Pshenichnikov, M. S.; Hummelen, J. C. *Nature Photon* **2012**, *6*, 560. (h) van der Ende, B. M.; Aartsa, L.; Meijerink, A. *Phys. Chem. Chem. Phys.* **2009**, *11*, 11081. (i) Huang, X.; Han, S.; Huang, W.; Liu, X. *Chem. Soc. Rev.* **2013**, *42*, 173. (j) Xie, X.; Liu, X. *Nat. Mater.* **2012**, *11*, 842. (k) Xu, H.; Wang, L. H.; Zhu, X. H.; Yin, K.; Zhong, G. Y.; Hou, X. Y.; Huang, W. *J. Phys. Chem. B* **2006**, *110*, 3023. (l) Li, C.; Lin, J. *J. Mater. Chem.* **2010**, *20*, 6831. (m) Xu, H.; Yin, K.; Huang, W. *J. Phys. Chem. C* **2010**, *114*, 1674. (n) Teng, X.; Zhu, Y.; Wei, W.; Wang, S.; Huang, J.; Naccache, R.; Hu, W.; Tok, A. I. Y.; Han, Y.; Zhang, Q.; Fan, Q.; Huang, W.; Capobianco, J. A.; Huang, L. *J. Am. Chem. Soc.* **2012**, *134*, 8340. (o) Wang, G.; Peng, Q.; Li, Y. *Acc. Chem. Res.* **2011**, *44*, 322. (p) Zheng, W.; Zhu, H.; Li, R.; Tu, D.; Liu, Y.; Luo, W.; Chen, X. *Phys. Chem. Chem. Phys.* **2012**, *14*, 6974. (q) Liu, Y.; Tu, D.; Zhu, H.; Li, R.; Luo, W.; Chen, X. *Adv. Mater.* **2010**, *22*, 3266. (r) Tu, D.; Liu, L.; Ju, Q.; Liu, Y.; Zhu, H.; Li, R.; Chen, X. *Angew. Chem., Int. Ed.* **2011**, *50*, 6306. (s) Li, C.; Yang, J.; Quan, Z.; Yang, P.; Kong, D.; Lin, J. *Chem. Mater.* **2007**, *19*, 4933.

(5) (a) Shen, J.; Sun, L.; Yan, C. *Dalton Trans.* **2008**, 5687. (b) Wang, F.; Banerjee, D.; Liu, Y.; Chen, X.; Liu, X. *Analyst* **2010**, *135*, 1839. (c) Zhou, J.; Liu, Z.; Li, F. *Chem. Soc. Rev.* **2012**, *41*, 1323. (d) Bünzli, J-C. G. *Chem. Rev.* **2010**, *110*, 2729. (e) Mader, H. S.; Kele, P.; Saleh, S. M.; Wolfbeis, O. S. *Curr. Opin. Chem. Biol.* **2010**, *14*, 582. (f) Barreto, J. A.; O'Malley, W.; Kubeil, M.; Graham, B.; Stephan, H.; Spiccia, L. *Adv. Mater.* **2011**, *23*, H18.

(6) (a) Heer, S.; Kömpe, K.; Güdel, H.-U.; Haase, M. *Adv. Mater.* **2004**, *16*, 2102. (b) Vetrone, F.; Mahalingam, V.; Capobianco, J. A. *Chem. Mater.* **2009**, *21*, 1847. (c) Yang, L.; Han, H.; Zhang, Y.; Zhong, J. *J. Phys. Chem. C* **2009**, *113*, 18995. (d) Chen, D.; Yu, Y.; Huang, F.; Huang, P.; Yang, A.; Wang, Y. *J. Am. Chem. Soc.* **2010**, *132*, 9976. (e) Chan, E. M.; Han, G.; Goldberg, J. D.; Gargas, D. J.; Ostrowski, A. D.; Schuck, P. J.; Cohen, B. E.; Milliron, D. J. *Nano Lett.* **2012**, *12*, 3839.

(7) (a) Wong, H.-T.; Chan, H. L. W.; Hao, J. *Opt. Express* **2010**, *18*, 6123. (b) Wang, J.; Wang, F.; Xu, J.; Wang, Y.; Liu, Y.; Chen, X.; Chen, H.; Liu, X. *C. R. Chim.* **2010**, *13*, 731. (c) Zeng, S.; Ren, G.; Li, W.; Xu, C.; Yang, Q. *J. Phys. Chem. C* **2010**, *114*, 10750. (d) Chen, G.; Qiu, H.; Fan, R.; Hao, S.; Tan, S.; Yang, C.; Han, G. *J. Mater. Chem.* **2012**, *22*, 20190.

(8) (a) Wang, F.; Han, Y.; Lim, C. S.; Lu, Y.; Wang, J.; Xu, J.; Chen, H.; Zhang, C.; Hong, M.; Liu, X. *Nature* **2010**, *463*, 1061. (b) Wang, F.; Liu, X. *J. Am. Chem. Soc.* **2008**, *130*, 5642. (c) Chen, G.; Ohulchanskyy, T. Y.; Kumar, R.; Ågren, H.; Prasad, P. N. *ACS Nano* **2010**, *4*, 3163. (d) Wang, F.; Wang, J.; Xu, J.; Xue, X.; Chen, H.; Liu, X. *Spectrosc. Lett.* **2010**, *43*, 400.

(9) (a) Tian, G.; Gu, Z.; Zhou, L.; Yin, W.; Liu, X.; Yan, L.; Jin, S.; Ren, W.; Xing, G.; Li, S.; Zhao, Y. *Adv. Mater.* **2012**, *24*, 1226. (b) Wang, J.; Wang, F.; Wang, C.; Liu, Z.; Liu, X. *Angew. Chem., Int. Ed.* **2011**, *50*, 10369. (c) Zhang, Y.; Lin, J.; Vijayaragavan, V.; Bhakoo, K. K.; Tan, T. T. Y. *Chem. Commun.* **2012**, *48*, 10322.

(10) Wang, F.; Deng, R.; Wang, J.; Wang, Q.; Han, Y.; Zhu, H.; Chen, X.; Liu, X. *Nat. Mater.* **2011**, *10*, 968.

(11) Wang, F.; Wang, J.; Liu, X. *Angew. Chem., Int. Ed.* **2010**, *49*, 7456.

(12) Bogdan, N.; Vetrone, F.; Ozin, G. A.; Capobianco, J. A. *Nano Lett.* **2011**, *11*, 835.

(13) (a) Mai, H.; Zhang, Y.; Sun, L.; Yan, C. *J. Phys. Chem. C* **2007**, *111*, 13721. (b) Qian, H.-S.; Zhang, Y. *Langmuir* **2008**, *24*, 12123. (c) Liu, X.; Kong, X.; Zhang, Y.; Tu, L.; Wang, Y.; Zeng, Q.; Li, C.; Shi, Z.; Zhang, H. *Chem. Commun.* **2011**, *47*, 11957. (d) Chen, D.; Lei, L.; Yang, A.; Wang, Z.; Wang., Y. *Chem. Commun.* **2012**, *48*, 5898. (e) Johnson, N. J. J.; Korinek, A.; Dong, C.; van Veggel, F. C. J. M. *J. Am. Chem. Soc.* **2012**, *134*, 11068. (f) Zhang, F.; Che, R.; Li, X.; Yao, C.; Yang, J.; Shen, D.; Hu, P.; Li, W.; Zhao, D. *Nano Lett.* **2012**, *12*, 2852. (g) Yi, G.; Chow, G. M. *Chem. Mater.* **2007**, *19*, 341. (h) Schäfer, H.; Ptacek, P.; Zerzouf, O.; Haase, M. *Adv. Funct. Mater.* **2008**, *18*, 2913.

(14) Zhang, S. *Spectroscopy of Rare Earth Ions*; Science Press: Beijing, 2008.

(15) Blasse, G.; Kiliaan, H. S.; De Vries, A. J. *J. Less-Common Met.* **1986**, *126*, 139.
(16) Qian, L.; Yuan, D.; Yi, G.; Chow, G. M. *J. Mater. Res.* **2009**, *24*, 3559.
(17) Kellendonk, F.; Blasse, G. *J. Phys. Chem. Solids* **1982**, *43*, 481.
(18) Blasse, G. *Phys. Lett. A* **1968**, *28*, 444.
(19) Komban, R.; Klare, J. P.; Voss, B.; Nordmann, J.; Steinhoff, H.-J.; Haase, M. *Angew. Chem., Int. Ed.* **2012**, *51*, 6506.